

# Ionic Polymer-Metal Composite Coated with Polyaniline Film by Electrodeposition: A Promising IPMC/PANI Junction for Applications in Robotics and Bioengineering

Cristiano Porporatti Zimmermann<sup>a</sup>, Gabriela Madella Kranz<sup>b</sup>, João Paulo Eckert<sup>c</sup>, Lucas Fadani<sup>c</sup>,  
Micheli Zanetti<sup>b,c</sup>, Josiane Maria Muneron de Mello<sup>b,c,d</sup> , Paulo Roberto Innocente<sup>e</sup>,  
Gustavo Lopes Colpani<sup>b,c,d</sup> , Márcio Antônio Fiori<sup>e</sup>, Carlos Henrique Scuracchio<sup>a,\*</sup> 

<sup>a</sup>Universidade Federal de São Carlos, Programa de Pós-Graduação em Ciência e Engenharia de Materiais, Rod. Washington Luiz, Km 235, 13565-905, São Carlos, SP, Brasil.

<sup>b</sup>Universidade Comunitária da Região de Chapecó, Programa de Pós-Graduação em Tecnologia e Gestão da Inovação, Servidão Anjo da Guarda, 295 D, 89809-900, Chapecó, SC, Brasil.

<sup>c</sup>Universidade Comunitária da Região de Chapecó, Escola Politécnica, Engenharia Química, Servidão Anjo da Guarda, 295 D, 89809-900, Chapecó, SC, Brasil.

<sup>d</sup>Universidade Comunitária da Região de Chapecó, Programa de Pós-Graduação em Ciências Ambientais, Servidão Anjo da Guarda, 295 D, 89809-900, Chapecó, SC, Brasil.

<sup>e</sup>Universidade Tecnológica Federal do Paraná, Departamento de Física, Via do Conhecimento, Km 01, 85503-390, Pato Branco, PR, Brasil.

Received: December 18, 2022; Revised: March 21, 2023; Accepted: April 14, 2023

Ionic polymer-metal composites (IPMC) are typical electromechanical transducing materials suitable for use as soft actuators, bioinspired artificial muscles and sensors. However, IPMC produced with platinum films has the great disadvantage of the large number of cracks and wrinkles, which reduce the performance of the electrode. Polyaniline (PANI) is a promising conductive polymer that can address this issue, especially when it is electropolymerized on the platinum surface. An IPMC/PANI actuator was developed by potentiostatic electropolymerization of PANI at 0.9 V in 0.1 M and 0.3 M aniline solution. The characterization revealed that PANI is preferentially electropolymerized in the platinum film cracks and improve the electronic conduction mechanisms, which is not reported so far. The maximum tip displacement of the IPMC/PANI under 5 V was 8.3 mm, while for the IPMC was equal 5.2 mm. These results provide a simple and effective method to repair IPMCs and enhance their electromechanical performances.

**Keywords:** Polyaniline, platinum, Nafion, electromechanical response, impedance, electropolymerization.

## 1. Introduction

Ionic polymer-metal composites (IPMC) are a class of electroactive polymer composites formed by an ion-exchange membrane coated with metal electrode layers at both sides<sup>1,2</sup>, which have been considered as a promising candidate to be used in actuators, bioinspired artificial muscles and sensors<sup>3</sup> because of their advantageous properties like large deformation in the presence of low applied voltage, low weight, flexibility, softness, low power consumption, rapid response and mechanical and chemical tolerance and stability<sup>4-7</sup>. However, IPMC tends to form cracks and wrinkles that decrease electric conductivity of the electrode, cause significant water leakage and loss of electromechanical response principally on the surface<sup>8-10</sup>. To overcome these disadvantages and optimize time and cost of manufacturing, as well as increase the reliability of the composite, many researches are committed to obtaining a flexible electrode with stable actuation performance. Conductive polymer surface coatings are attracting special attention because

they can modify the electrode surface chemistry and increase the mechanical strength of one<sup>11,12</sup>. Conductive polymers such as polypyrrole (PPY)<sup>13,14</sup>, poly(ethylenedioxythiophene) (PEDOT)<sup>15,16</sup> and polyaniline (PANI)<sup>17</sup> are attractive materials for coating IPMC due to unique properties. Polyaniline is considered as one of the most promising conducting polymer due to its wide variation of conductivity, tunable redox behavior, environmental and electrochemical stability, facile synthesis and low cost<sup>18,19</sup>. In this study, a PANI coated IPMC has been developed through electroless platinum deposition and then potentiostatic electrodeposition method. The electrochemical results showed that it is possible to obtain regular films of PANI on the IPMC surface by potentiostatic conditions. After electrodynamic tests, the IPMC/PANI junctions showed an enhance on the displacement due to an improvement on the charge distribution on the electrode membrane, a promising result for the development of devices with better electromechanical responses, considering the relative simplicity of the electrode coating method.

\*e-mail: carlos.scu@ufscar.br

## 2. Materials and Methods

### 2.1. Materials

Nafion® membrane ( $[\text{C}_7\text{HF}_{13}\text{O}_5\text{S-C}_2\text{F}_4]_x$ , N-117, thickness: 178  $\mu\text{m}$ ), used as polyelectrolyte of IPMC actuators, was purchased from Sigma Aldrich. Hydrogen peroxide ( $\text{H}_2\text{O}_2$  – 35% volume, Dinâmica) and ammonium hydroxide ( $\text{NH}_4\text{OH}$  – ACS grade) were purchased from Dinâmica and sulfuric acid ( $\text{H}_2\text{SO}_4$  – ACS grade), aniline ( $\text{C}_6\text{H}_5\text{NH}_2$  – 99.5%), hydrochloric acid ( $\text{HCl}$  – 37%), tetraammineplatinum chloride ( $[\text{Pt}(\text{NH}_3)_4]\text{Cl}_2$  – 98%), sodium borohydride ( $\text{NaBH}_4$  – 98%) and sodium sulfate ( $\text{Na}_2\text{SO}_4$  – ACS grade) were purchased from Sigma-Aldrich.

### 2.2. IPMC sample preparation

A traditional reduction-plating method<sup>20-22</sup> was used to prepare the IPMC samples, as observed in the schematic illustration in Figure 1. The as-prepared membrane was submerged in a beaker containing  $\text{H}_2\text{O}_2$  5% (v/v) for 60 min at 70 °C for elimination of organic impurities. Then, all membranes were immersed in 1 M HCl aqueous solutions at 70 °C for 30 min, in order to impregnate  $\text{H}^+$  ions, and cleaned in water at 65–70 °C for 30 min to remove acid residue.

The Nafion® samples were immersed in aqueous solution of  $\text{Pt}(\text{NH}_3)_4\text{Cl}_2$  (3 mg of Pt per  $\text{cm}^2$ ) and  $\text{NH}_4\text{OH}$  (5% v/v) for 48 h at room temperature to allow ion exchange of  $[\text{Pt}(\text{NH}_3)_4]^{2+}$  with  $\text{H}^+$  of membrane and the platinum complex diffusion. Electroless reduction of Pt ions on the membrane

surface was performed with 5 wt% aqueous solution of  $\text{NaBH}_4$  as a reducing agent. The samples were submerged in a deionized water bath at 60 °C under magnetic stirring and 3.3 ml  $\text{NaBH}_4$  solution were added dropwise every 20 min for 5 times until the reagent was proportional to the area of the membrane. Then, IPMC samples were rinsed with deionized water and dried at room temperature.

After sample preparation, counter-ions were exchanged into the membrane through a cation exchange process. In order to prepare IPMC with  $\text{H}^+$ , samples were immersed in HCl (1 M) solution for 24 h and sliced in stripes with 15 x 5 mm.

### 2.3. Electropolymerization of PANI on IPMC surface

The electrochemical polymerization of aniline (cyclic voltammetry and chronoamperometry) was performed according to previous work<sup>23-25</sup> using a potentiostat and galvanostat (Methrom, AUTOLAB PGSTAT 204) connected to a personal computer. All electrochemical measurements were carried out at room temperature (25 °C) in a standard three-electrode Pyrex-glass cell (100 ml) containing platinum plate as counter electrode, saturated calomel electrode (SCE) as reference electrode and the IPMC as working electrode. The electrolyte solution was 1.0 M  $\text{H}_2\text{SO}_4$  aqueous solution containing different concentrations of aniline (0.1 and 0.3 M). Firstly, the electropolymerization of aniline on the IPMC electrodes was performed by cyclic voltammetry (CV) with a scan rate of 50  $\text{mV}\cdot\text{s}^{-1}$  between -0.1 and 1.5 V (vs. SCE) for 4 cycles to avoid the onset potentials of hydrogen and oxygen evolution<sup>26-28</sup>.

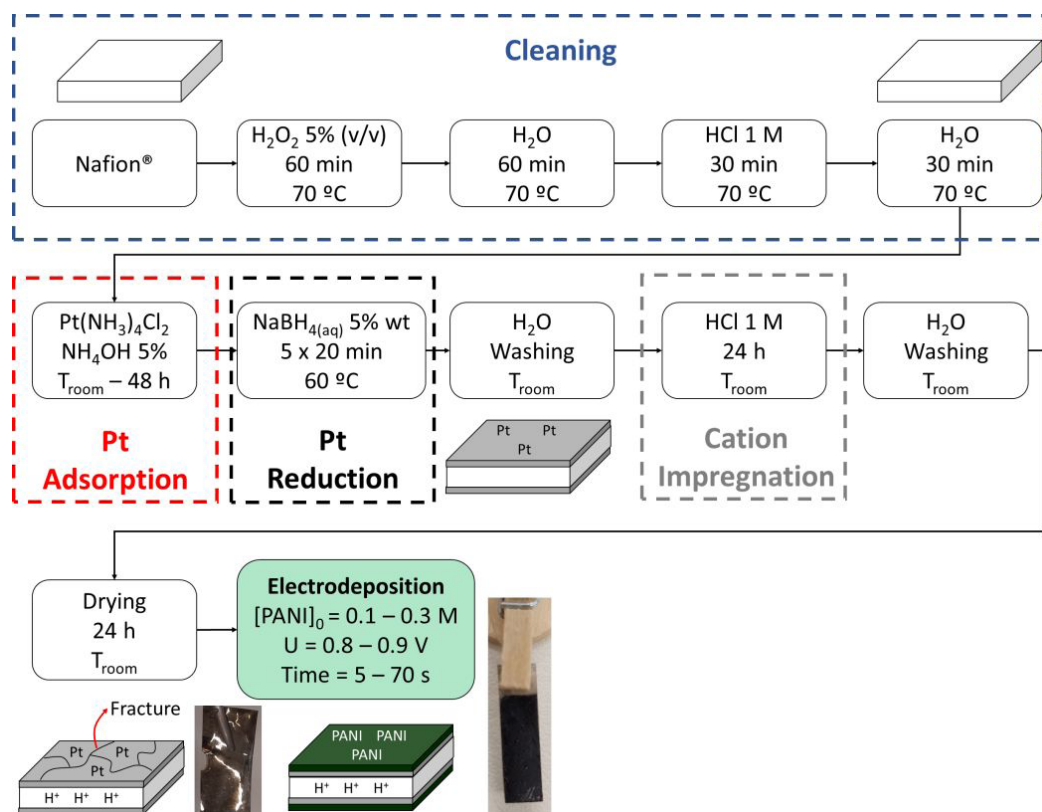


Figure 1. Schematic illustration of IPMC/PANI sample preparation.

Then, a chronoamperometric (CA) method was carried out to evaluate the electropolymerization mechanism of aniline at 0.9 V (vs. SCE). This potential was determined from the first appeared anodic peak in CV experiments. For the CA tests, the electrochemical polymerization of PANI films was recorded at  $50 \text{ mV}\cdot\text{s}^{-1}$  during 15 s and 20 s using an aqueous solution of 1.0 M  $\text{H}_2\text{SO}_4$  and aniline (0.1 and 0.3 M). After deposition, the films were washed with deionized water and stored in a desiccator at room temperature.

#### 2.4. Characterization

Electrochemical impedance spectroscopy (EIS) was performed at 1.2 V (vs. SCE) using 0.1 M  $\text{Na}_2\text{SO}_4$  aqueous solution as an electrolyte. EIS measurements were carried out under open-circuit voltage with an ac signal (amplitude equal 5 mV) in the frequency range of 0.1 Hz to  $10^6$  Hz. The impedance analysis was carried out using the Nyquist and Bode plots. The resultant impedance spectra were simulated using the Origin 8.5 software.

As depicted in Figure 2, all IPMC tip deflection measurements were carried out in a closed acrylic chamber with relative humidity near 85%, which is similar to that developed by Saccardo et al.<sup>7</sup>. The humidity was increased using water vapor generated by an ultrasonic nebulizer. Inside this chamber, one analog humidity sensor (RHT-P10, Novus) measured the relative humidity (RH) and temperature. The actual bending at the tip was measured by a laser displacement sensor (IL-030, Keyence) 55 mm from the edge of the IPMC tip. The system used for control and data acquisition is composed of a programmable logic controller (1769-L24ER-QBFC1B CompactLogix 5370 Controller - Rockwell Automation/Allen-Bradley) and a supervisory system developed in the FTView Studio (Rockwell Automation). The IPMC and IPMC/PANI samples have been subjected to input a direct current voltage equal  $5 \text{ V}_{\text{DC}}^{29,30}$ , applied by a power source model (iCel, PS-4000) during 180 s.

The samples (15 x 5 mm) were clamped at one end between two parallel stainless steel wires (with a plastic clothespin as support) in a cantilever configuration, while the other end was subject to bend horizontally by applied voltage.

Scanning electron microscopy (FEI Magellan 400 L) was performed to observe the surface and cross-sectional morphology of the IPMC/PANI electropolymerized at 0.9 V in 0.3 M aniline at different times (15 and 20 s). The samples were examined under high voltage (20 kV) at different magnifications. To obtain the cross section the samples were cryogenically fractured in liquid nitrogen and sputtered with gold before viewing. EDS analyzes on the surface of IPMC and IPMC/PANI were performed by energy-dispersive X-ray spectroscopy mapping (INCA X Sight 6650X) to investigate the elemental composition on the surface of the samples in the energy range of 0–18 keV and 20 kV accelerating voltage.

The FTIR (Frontier Perkin Elmer) spectra of IPMC and IPMC/PANI were recorded from 4000 to  $400 \text{ cm}^{-1}$  at room temperature.

### 3. Results and Discussions

#### 3.1. Cyclic voltammetry

The electropolymerization was performed in an aqueous solution containing aniline (0.1 or 0.3 M) and  $\text{H}_2\text{SO}_4$  1 M as inorganic dopant, because polyaniline prepared in sulfuric acid solutions is more conductive<sup>31</sup>. The electrodeposition process was performed using cyclic voltammetry (CV) scans and the results are shown in Figure 3. It can be seen the onset of oxidation occurs at 0.7 V (vs. SCE) in the first cycle and at a markedly lower potential in the others cycles, about 0.2 V. The anodic peak around 1.2 V that appeared at the first cycle is due to the oxidation of monomer to form cation radicals<sup>32</sup>. The increase in the peaks after 4 cycles indicates the formation of PANI film on the surface of the IPMC and that the film obtained is electrochemically active<sup>33</sup>.

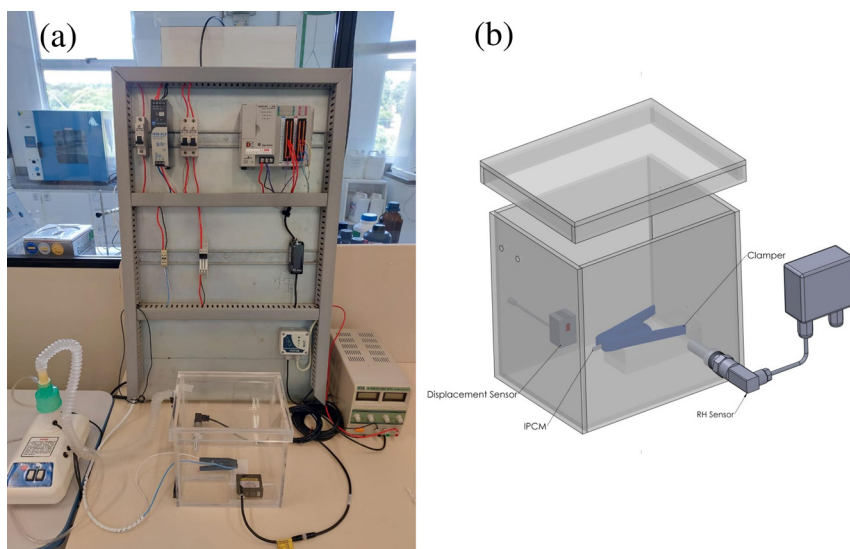
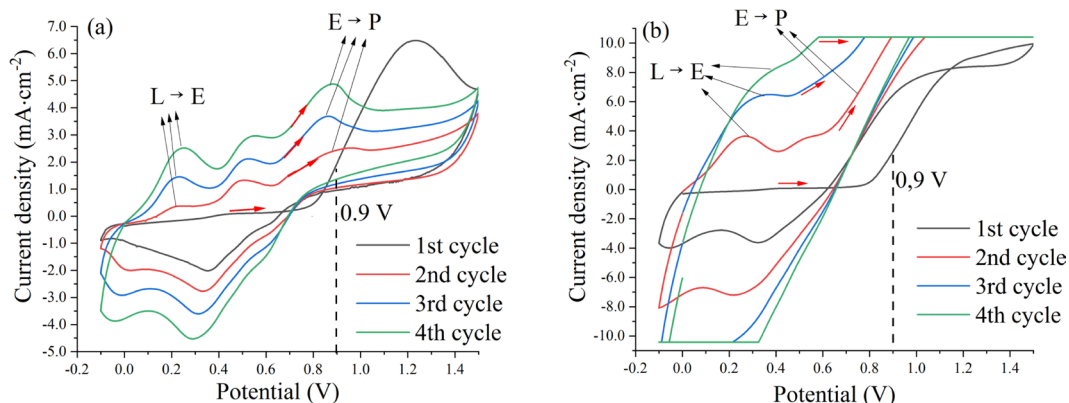


Figure 2. Experimental setup for tip deflection measurements (a) and acrylic chamber details (b).



**Figure 3.** Cyclic voltammogram of IPMC/PANI electrodes during electropolymerization in 1.0 M  $\text{H}_2\text{SO}_4$  solution containing (a) 0.1 M aniline and (b) 0.3 M aniline.

Moreover, the voltammograms (2<sup>nd</sup>, 3<sup>rd</sup> and 4<sup>th</sup> cycles) show the typical PANI oxidation with an anodic peak at approximately 0.2 V (vs. SCE) corresponding to the oxidation of leucoemeraldine (reduced form – yellow) to emeraldine (partially reduced form – green) form and a peak around 0.9 V related to the oxidation of emeraldine to the completely oxidized form pernigraniline<sup>34,35</sup>. From cyclic voltammetry results, a potential equal 0.9 V (vs. SCE) was selected to electropolymerize PANI under potentiostatic control. The selected potential was close to the aniline oxidation, which was determined from the first appeared anodic peak as shown in the first cycle.

### 3.2. Electropolymerization of PANI by chronoamperometry

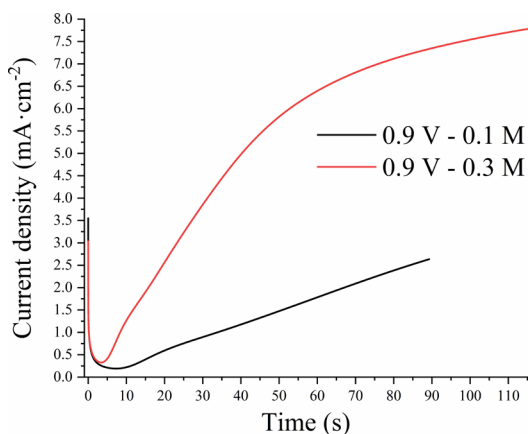
Figure 4 illustrates the chronoamperometric curves recorded during the electrochemical deposition of PANI (0.1 and 0.3 M) at 0.9 V. A current-transient showing three stages was obtained during aniline oxidation. In the first one there is a sudden drop in current density due to the depletion of charges at the electrical double layer because the rapid consumption of aniline (near the surface of the IPMC) and diffusion-controlled process during the initial phase of the reaction<sup>35-38</sup>.

During the second stage there is an increase in current due to aniline oxidation along with nucleation of the polymer, film growth in two dimensions and polyaniline deposition at the anode surface. Finally, in the last stage the current densities gradually increase due to the growth polymerization of the second layer of PANI over the first one<sup>38-41</sup>. After electropolymerization, a dark green film can be seen on the IPMC surface.

As shown in Figure 4 it can be seen clearly that the electropolymerization behavior was dependent on the electroactive species concentration. From chronoamperometric curves, the IPMC/PANI samples were synthesized at the deposition potential of 0.9 V and the electropolymerization time of 20 s for the subsequent experiments. These values were chosen to avoid films with high thickness.

### 3.3. Scanning electron microscopy

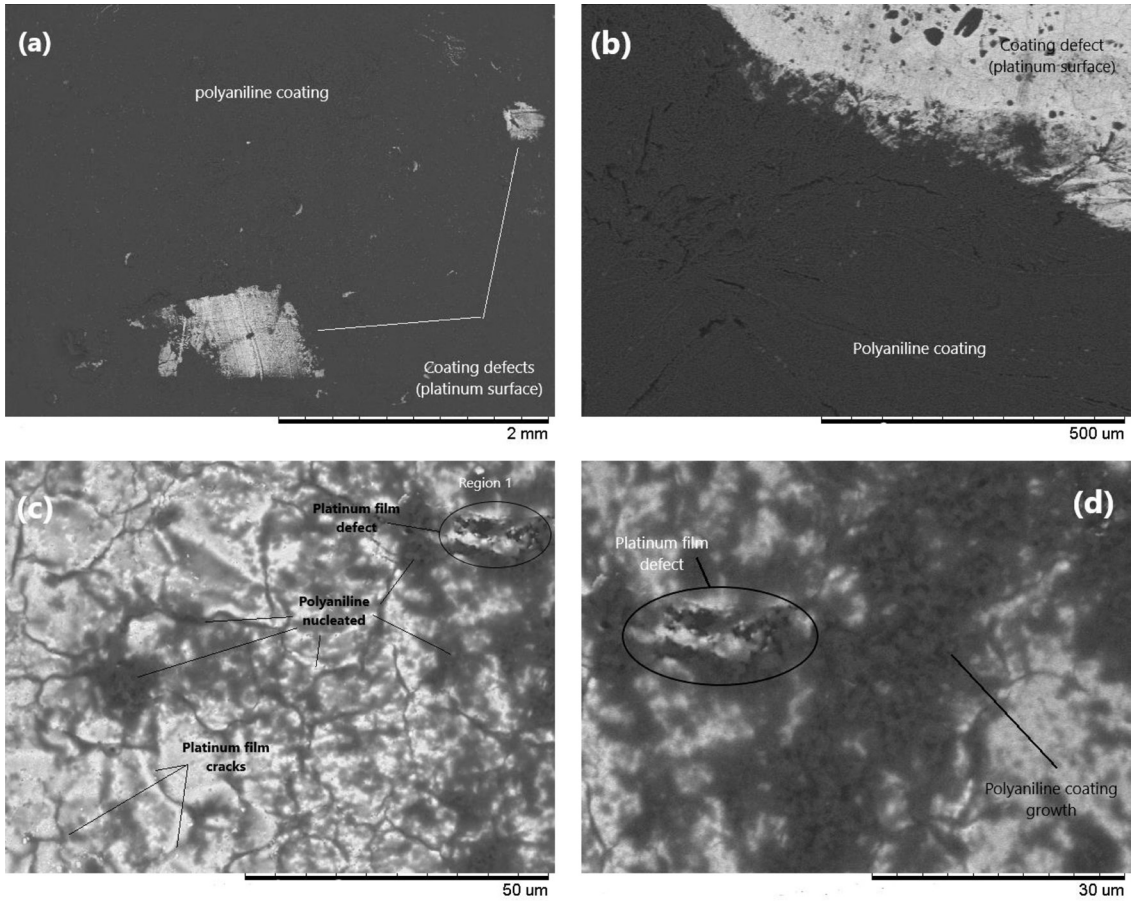
Figure 5 shows SEM images of IPMC surfaces coated with polyaniline electropolymerized in 0.30 M aniline solution



**Figure 4.** Chronoamperometric curves recorded for electropolymerization of aniline on IPMC in a 1.0 M  $\text{H}_2\text{SO}_4$  aqueous solution at 0.9 V.

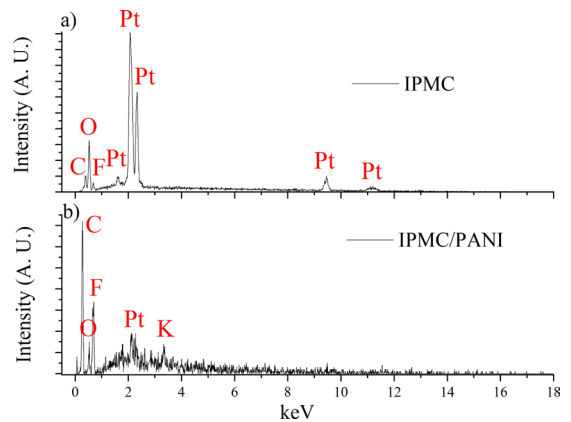
at 0.90 V during 15 seconds. A regular PANI film is formed on the IPMC platinum electrode surface, but with some coating defects that expose the platinum surface, as shown in Figure 5a. These defects are to be expected considering that the curing time of 15 seconds is normally not sufficient for complete surface coverage. Details of the SEM images show that the PANI coating is quite thick, to the point of forming surface cracks due to internal stresses (Figure 5b).

Figure 5c shows details of a platinum region with a PANI coating defect. The images show that the platinum coating on the IPMC surface has many cracks, similar to the platinum IPMC coatings obtained by Gonçalves et al.<sup>42</sup>. However, it is clear that PANI is preferentially electropolymerized in these platinum film defects (cracks). This characteristic is due to the fact that the values of the electric field at the edges of these cracks are greater (peak effect for the electric field) during the electropolymerization process and, therefore, the mechanisms of electric charge transfer are favored and the rates of electropolymerization are greater in these regions and, therefore, the nucleation of the polyaniline grains occurs preferentially and more quickly in these cracked regions of the platinum film. In this way, the nucleation process of the PANI films begins in the cracks of the platinum electrodes.



**Figure 5.** SEM images of IPMC surfaces coated with polyaniline electropolymerized with the 0.30 M PANI solution, an electrical potential of 0.90 V and 15 seconds. (a) magnification 40 times, (b) magnification 180 times, (c) magnification 1800 times and (d) magnification 2500 times.

A magnification of the image in Region 1 (Figure 5c) is shown in Figure 5d. It is evident that the cracks in the platinum films are filled by polyaniline molecules, to the point of filling the defects of the platinum film in the IPMC electrode. Although polyaniline is less conductive than platinum films, it is still an electrically conductive material. It is then expected that, with the filling of the cracks by PANI, the number of defects in the IPMC electrode will be reduced. As the fractures act as scattering centers of charge carriers in the electronic conduction process, the reduction in the number of these centers, due to the polyaniline filling, favors the electronic conduction mechanisms and provides an increase in the effective area of electronic charging of the IPMC. Also, with the reduction of the scattering centers of charge carriers, it is likely that the distribution of charges on the surface of the IPMC electrode (Platinum + PANI) will be more uniform. Therefore, filling these cracks with PANI should favor a larger and more uniform electric field and a larger effective electrode area for the IPMC Nafion® core<sup>43</sup>. The EDS spectra of the IPMC and IPMC/PANI are shown in Figure 6 and revealed the characteristic elemental peaks of carbon, oxygen, fluoride, which are the basic elements of pure Nafion®, and platinum. The Pt represents the highest peak in Figure 6a, showing an excellent deposition of the metal electrode at the surface of the membrane actuator.



**Figure 6.** EDS spectra of (a) IPMC and (b) IPMC/PANI.

From the peaks in the EDS analysis of IPMC/PANI, depicted in Figure 6b, after polyaniline electrodeposition, it is clear that the amount of carbon in the sample sharply increases. At the same time, the percentage of Pt decreases, which is attributed to the formation of PANI coating on the surface of IPMC. Table 1 represents the mass percentage of the elements for different samples.

An image on the edge of the polyaniline coating of the platinum film with a longer electropolymerization time (15 seconds) shows the formation of a regular polyaniline film and the absence of significant defects. The polyaniline coating is a uniform film and covers the entire platinum film and its defects, as depicted in Figure 7a. SEM-BSE image obtained with a backscattering detector of a polyaniline-coated IPMC cross-section is shown in Figure 7b and a PANI grain coated on the IPMC platinum film surface can be observed. The image reveals a platinum film with a thickness of around 1  $\mu\text{m}$  and its defects (cracks) and a PANI grain with a thickness of around 2  $\mu\text{m}$ . Figure 7c shows an SEM-BSE image at higher magnification and reveals the filling of cracks in the platinum film by the polyaniline coating.

Thus, the SEM studies confirm that from the electropolymerization it is possible to obtain a uniform polyaniline film on the platinum film and to fill in the platinum defects (cracks in the platinum coating of the IPMC).

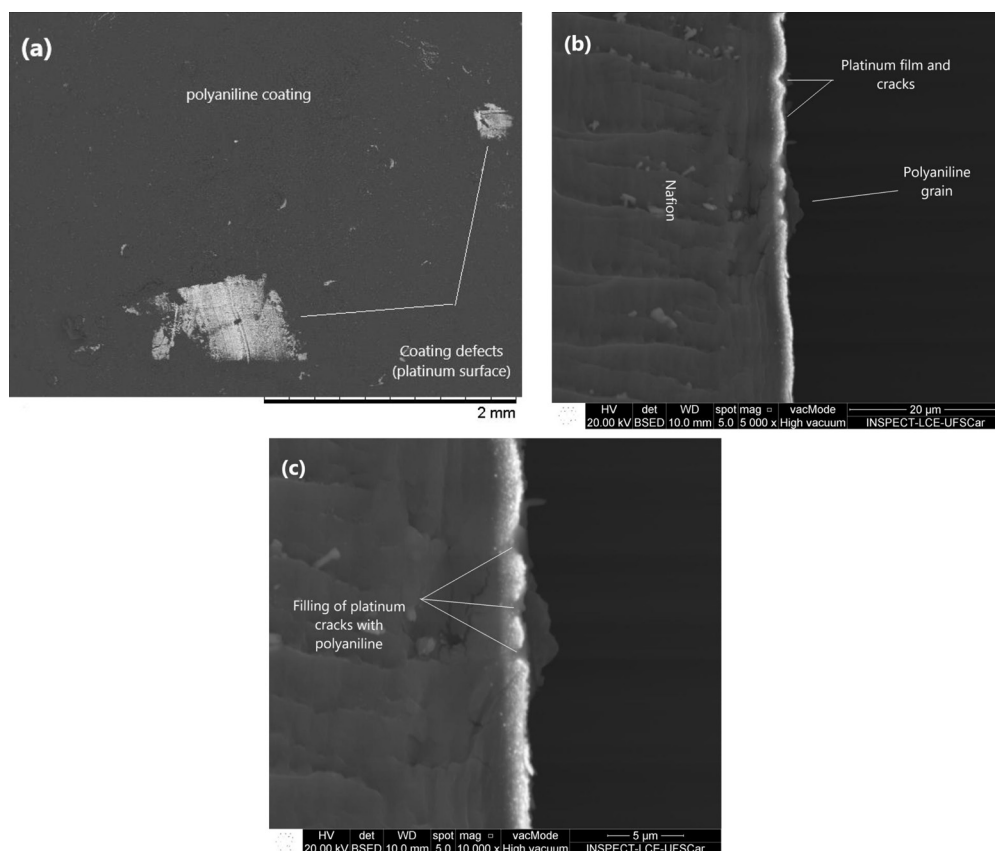
### 3.4. Fourier transformed infrared spectroscopy analyzes

Figure 8 depicts the FTIR spectra for the IPMC and IPMC/PANI film. In comparison with the IPMC membrane, the electropolymerized sample shows new peaks related to polyaniline. The characteristic absorption peak of stretching mode of the N–H bond appears at  $3217\text{ cm}^{-1}$ , indicating the existence of secondary amine unit of PANI on the IPMC surface<sup>44</sup>. The peaks at  $1558\text{ cm}^{-1}$  and  $1484\text{ cm}^{-1}$  suggest the non-symmetric vibration of C–H bonds in the quinoid rings and C=C stretching mode of benzenoid rings of the partially reduced form of PANI, respectively<sup>44-46</sup>. The peak at  $1290\text{ cm}^{-1}$  corresponds to  $\pi$ -electron delocalization resulting from the protonation of the polyaniline<sup>46</sup>. The absorption bands at  $1108\text{ cm}^{-1}$  and  $1048\text{ cm}^{-1}$  are attributed to the substituted benzene ring<sup>47-49</sup>.

**Table 1.** Elemental composition from the surfaces of IPMC and IPMC/PANI.

Sample	C		O		F		Pt		K	
	wt.%	at.%	wt.%	at.%	wt.%	at.%	wt.%	at.%	wt.%	at.%
IPMC	1.01	4.58	12.72	43.13	1.30	3.70	67.31	18.71	ND	ND
IPMC/PANI	53.01	67.11	9.76	9.27	25.22	20.19	5.08	0.40	4.76	1.85

ND – Not detected



**Figure 7.** SEM images of IPMC surfaces coated with polyaniline electropolymerized with the 0.30 M PANI solution, an electrical potential of 0.90 V and 15 seconds. (a) formation of a regular polyaniline film and the absence of significant defects, (b) image obtained with a BSE detector of a polyaniline-coated IPMC cross-section and (c) SEM-BSE image at higher magnification.

### 3.5. Electrochemical impedance spectroscopy (EIS) investigation

Electrochemical impedance measurements were carried out to investigate the behavior of electronic conduction processes in the IPMC/PANI and to determine the equivalent electronic circuit and its respective parameters. The impedance spectra in the form of Nyquist and Bode plots for IPMC/PANI are given in Figure 9. These impedance plots were modeled by the equivalent circuit inserted in Figure 9b.

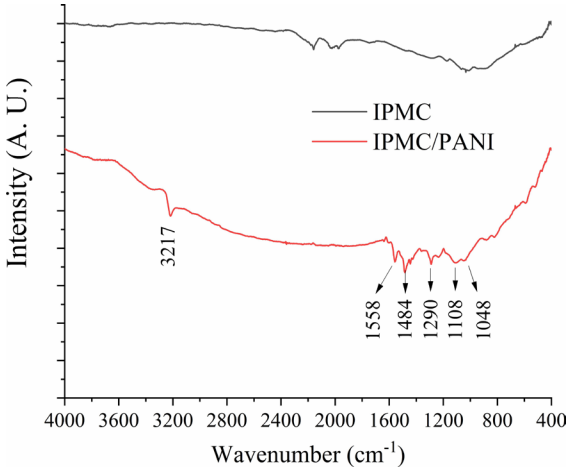
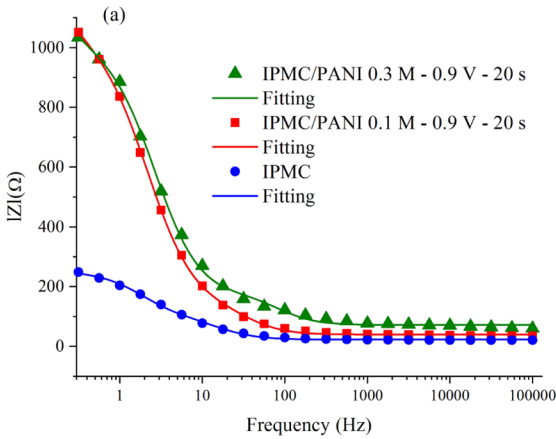


**Figure 8.** FTIR for IPMC and IPMC/PANI samples between the wavenumber from 4000 to 400  $\text{cm}^{-1}$ .



The equivalent circuit consists of the electrolyte resistance ( $R_s$ ), film resistance ( $R_f$ ), film capacitance ( $C_f$ ), charge transfer resistance ( $R_{ct}$ ), double layer capacitance ( $C_{dl}$ ) and the Warburg impedance element ( $Z_d$ ) for the IPMC/PANI, whereas the last one is a complex factor that depends of the frequency and is calculated according to the Equation 1. The  $Z_d$  parameter is commonly used to represent diffusion controlled charge transfer process in pseudo-capacitors<sup>50,51</sup>. This agrees with the fact that PANI has high pseudocapacitive performance<sup>52</sup>.

$$Z_d = \sigma \cdot \omega^{-\frac{1}{2}} \cdot (1 - j) \quad (1)$$

where  $\sigma$  is the Warburg impedance coefficient associated with the diffusivity in the electronic system,  $\omega$  is the angular frequency and  $j$  is the imaginary unit ( $-1^{1/2}$ ).

The impedance parameters for the IPMC/PANI acquired using Origin 8.5 software are given in Table 2 and the Bode plots depicted in Figure 9a were fitted with the parameters of the equivalent circuit in the whole frequency range. The semi-circle in the Nyquist plot, as illustrated in Figure 9b is attributed to the charge-transfer resistance mechanisms in the IPMC/PANI ( $R_{ct}$ )<sup>53</sup>. Thus, the high  $R_{ct}$  value of the IPMC/PANI suggests that this actuator has a lower transfer rate of electronic carriers compared to the IPMC without the PANI coating and lower values of electric current<sup>53,54</sup>. The lower electric current implies a longer time for its electronic charging, but a lower thermal energy dissipation rate, which improves the performance of the IPMC<sup>13,17</sup>. The electropolymerized PANI grows on the IPMC surface and fills into the cracks of the platinum layer, which increases the effective area.

**Figure 9.** Electrochemical impedance spectra of (a) Bode and (b) Nyquist. The inset figure shows the equivalent circuit model for fitting the electrochemical impedance.

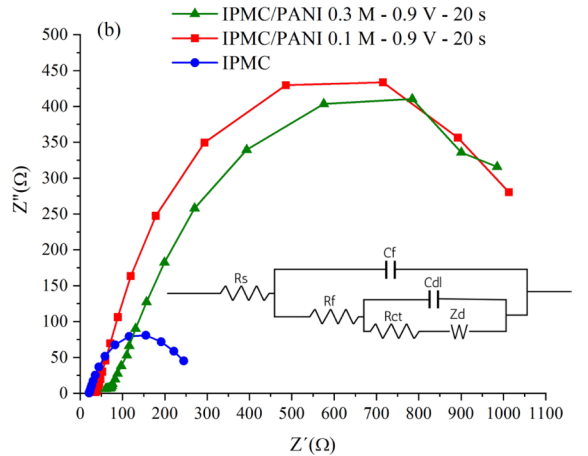


**Table 2.** Equivalent circuit parameters of the IPMC and IPMC/PANI obtained from EIS data fitting.

Sample	$R_s$ ( $\Omega$ )	$R_f$ ( $\Omega$ )	$R_{ct}$ ( $\Omega$ )	$C_f$ (F)	$C_{dl}$ (F)	$\sigma$ ( $\Omega \cdot \text{s}^{1/2}$ )
IPMC	22.8	109.8	102.9	$1.70 \cdot 10^{-4}$	$7.1 \cdot 10^{-4}$	23.5
IPMC/PANI 0.3 M - 0.9 V - 20 s	71.7	144.1	679.1	$2.1 \cdot 10^{-4}$	$8.4 \cdot 10^{-5}$	219.1
IPMC/PANI 0.1 M - 0.9 V - 20 s	39.1	176.5	638.0	$4.6 \cdot 10^{-4}$	$7.1 \cdot 10^{-5}$	334.0

Then, the stored charge at the Pt/PANI and Nafion® interface increase, according Equation 2, and was expected to enhance the bending response of the electrode.

$$q_d = \varepsilon \frac{A_{ef}}{\varphi_d} V_{dct} \quad (2)$$

where  $q_d$  is the charge stored in the diffusion interface region of the IPMC/PANI in the equilibrium,  $\varepsilon$  is the electric permittivity,  $A_{ef}$  is the effective electrode area and the  $\varphi_d$  effective distance of the diffusion region.

According to the equivalent electric circuit, during the electronic charging of the IPMC/PANI, the electric charge on the electrode available for polarization and definition of the diffusive regime of the Nafion® nucleus can be determined as a function of the charging time according Equation 3. Also, at equilibrium, the value of the electrical charge can be determined from Equation 3, as a function of the effective charging area of the IPMC/PANI electrode.

$$q_d(t) = V_{dct} C_d \left( 1 - e^{-\frac{t}{\tau_c}} \right) \quad (3)$$

$$\tau_c = (R_{ct} + R_d) \cdot C_d$$

where,  $t$  is the IPMC/PANI charging time,  $V_{dct}$  is the electrical potential difference between the two PANI/Pt interfaces involving the Nafion® core,  $\tau_c$  is the capacitive time constant of the IPMC/PANI,  $R_d$  and  $C_d$  are the electronic conduction resistance and the capacitance related to the electronic carrier storage capacity of the diffusion mechanisms in the IPMC/PANI (directly associated with the values of  $Z_d$  and  $\sigma$ ), respectively.

IPMC coating with PANI provided significant increases in  $R_f$  (electrode resistance) and  $C_f$  (electrode capacitance) values, which implies an increase in conduction resistance and an increase in charges stored in the PANI/Pt interface of the IPMC. Considering that it is intended to coat the IPMC with PANI but with the optimal conditions for conducting the charge carriers for the highest loading of the Pt/Nafion interface, the best PANI coating should be the one in which the films have the lowest  $R_f$  and  $C_f$  values. In particular, among the electrodes with electrochemical deposited PANI, the electropolymerization condition with 0.3 M, 0.9 V and 20s presented the lowest  $R_f$  and  $C_f$  values, as shown in Table 2.

Comparing the IPMC/PANI obtained with this electropolymerization condition with the IPMC without PANI, the values of  $\sigma$  and of  $R_{ct}$  are higher. Then, the capacitive time constant for the IPMC/PANI is greater and the critical loading time for the onset of deformation is expected to be greater than the IPMC without PANI.

Therefore, from these results, the IPMC/PANI electrodes electropolymerized in 0.3 M aniline under 0.9 V during 20 s were selected for tip displacement experiments.

### 3.6. Bending analysis of IPMC and IPMC/PANI

The displacement curve of the IPMC and IPMC/PANI junction and the bending response at 5 V are shown in Figure 10. From these results, it is deduced that PANI plays an important role in the actuation of IPMC. The bending and displacement rate were considerably increased after PANI coating on the actuator surface. The maximum displacement of the IPMC/PANI under 5 V was 8.3 mm, while for the as-prepared IPMC was equal 5.2 mm. Table 3 summarizes some IPMC modification methods for improving the displacement response.

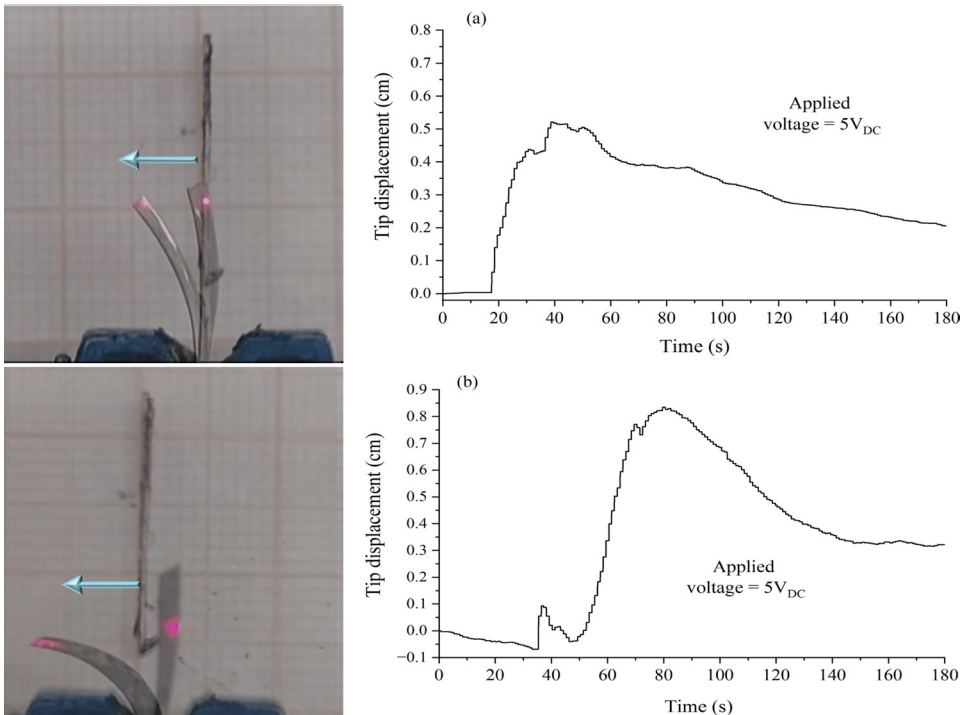


**Figure 10.** Tip displacement curves and images of (a) IPMC and (b) IPMC/PANI under 5  $V_{DC}$ .

**Table 3.** Performance comparison of different types of IPMC coated materials.

Sample	Materials	Electrode	Electrode coating method	Input DC Voltage (V)	Displacement (mm)	Ref.
IPMC/PANI	Nafion® film Polyaniline	Pt	Electropolymerization	5	8.3	This work
IPMC/PANI	Nafion® film Polyaniline	Graphene oxide	Dip coating	6.8	8.1	<sup>55</sup>
IP-PEDOT IP-PPY	Nafion® film PEDOT Polypyrrole Multi-wall carbon nanotube Carbon nanoparticle	Pt	Electropolymerization	5	19	<sup>13</sup>
				6	25	
PVDF/SGO/ PPY/Pt	PVDF Sulphonated graphene oxide Polypyrrole	Pt	Oxidative polymerization	5	14	<sup>12</sup>
SPVA-PANI	Sulfonated poly (vinyl alcohol), Polyaniline	Pt	Oxidative polymerization	5.25	14.5	<sup>56</sup>

With the application of external D.C. voltage, the  $H^+$  ions in IPMC migrate from the anode to the cathode and drag the water molecules along with them, which causes osmotic pressure change, and the IPMC bends toward the anode<sup>57,58</sup>. Therefore, it can be concluded that the PANI coated electrode had a significant improvement on the bending and displacement due to an improvement on the charge distribution on the electrode membrane<sup>59</sup> caused by the electropolymerization of aniline, which favors the electronic conduction mechanisms and provides an increase in the effective area of electronic charging of the IPMC, which is in agreement with the EIS and TEM analysis discussed below.

Moreover, the polyaniline electrodeposition on the IPMC implies an increase in the charge transfer resistance of electronic carriers, with an increase in the charging time, and the onset of deformation occurs later when compared with as-prepared IPMC, as can be seen in Figure 10.

Compared with uncoated IPMC, the actuator prepared with electrodeposited polyaniline has been found to show slower displacement speed and back relaxation. These results indicate that PANI formed very uniform structure and filled the IPMC defects, which allowed a more homogeneous charge distribution and led to a uniform electric field with higher magnitude in the IPMC.

#### 4. Conclusions

An IPMC actuator has been successfully prepared with polyaniline coating by electroless platinum deposition and potentiostatic electropolymerization method to fill the cracks and wrinkles of the platinum layer. The characterization analysis showed that the surface of IPMC was covered with PANI to the point of filling the defects of the platinum film in the IPMC electrode. As the fractures act as scattering centers of charge carriers in the electronic conduction process, the reduction in the number of these centers, favors the electronic conduction mechanisms. The incorporation of PANI in IPMC exhibited better resistance, capacitance and electromechanical performance compared with typical IPMC actuators,

probably due to an improvement on the charge distribution on the electrode membrane. The superior performance is a promising result to increase durability and repeatability of these actuators, which can expand the application in devices that require longer usage time.

#### 5. Acknowledgments

This work was financially supported by grants from Fundação de Amparo à Pesquisa do Estado de Santa Catarina (grant number 2021TR001929), Fundação de Amparo à Pesquisa do Estado de São Paulo (grant number 2018/07001-6) National Council for Scientific and Technological Development (CNPq – grant number 310076/2020-0), Coordenação de Aperfeiçoamento de Pessoal de Nível Superior (CAPES – grant number 23038.021524.2016.88) and Governo do Estado de Santa Catarina (UNIEDU). The authors acknowledge the Community University of Chapecó Region (Unochapecó), the Technological Federal University of the Paraná (UTFPR–PB) and the Structural Characterization Laboratory of Federal University of São Carlos (LCE - UFSCar) for technical and scientific support.

#### 6. References

1. He Z, Jiao S, Wang Z, Wang Y, Yang M, Zhang Y, et al. An antifatigue liquid metal composite electrode ionic polymermetal composite artificial muscle with excellent electromechanical properties. *ACS Appl Mater Interfaces*. 2022;14:14630-9.
2. Rasouli H, Naji L, Hosseini MG. Electrochemical and electromechanical behavior of Nafion-based soft actuators with PPy/CB/MWCNT nanocomposite electrodes. *RSC Advances*. 2017;7:3190-203.
3. Yin G, Yu M, Tong X, Wu Y, Tian C, Li Y. Fabrication and performance analysis of high performance cylindrical ionic polymer-metal composite actuators with various diameters. *Smart Mater Struct*. 2022. (In press).
4. Yang L, Zhang D, Zhang X, Tian A. Surface profile topography of ionic polymer metal composite based on fractal theory. *Surf Interfaces*. 2021;22:100834.
5. Ma S, Zhang Y, Liang Y, Ren L, Tian W, Ren L. High-performance ionic-polymer-metal composite: toward large-deformation fast-response artificial muscles. *Adv Funct Mater*. 2019;30(7):1908508.
6. Zhang M, Wang M, Zhang X, Zhang C, Li M, Yu S. Fabrication of a multilayered SGO/macroporous Nafion-based IPMC with

- enhanced actuation performance. *Sens Actuators B Chem.* 2022;356:131319.
7. Saccardo MC, Zuquello AG, Gonçalves R, Tozzi KA, Barbosa R, Hirano LA, et al. Electromechanical evaluation of ionomeric polymer-metal composites using video analysis. *Mater Res.* 2021;24(2):e20210317.
  8. He Q, Yin G, Vokoun D, Shen Q, Lu J, Liu X, et al. Review on improvement, modeling, and application of ionic polymer metal composite artificial muscle. *J Bionics Eng.* 2022;19:279-98.
  9. Wang F, Zhang X, Ma L, Zhang Z, Han L, Zeng C, et al. Facile and effective repair of Pt/Nafion IPMC actuator by dip-coating of PVP@AgNPs. *Nanotechnology.* 2021;32:385502.
  10. Guo D, Wang L, Wang X, Xiao Y, Wang C, Chen L, et al. PEDOT coating enhanced electromechanical performances and prolonged stable working time of IPMC actuator. *Sens Actuators B Chem.* 2020;305:127488.
  11. Khan A, Alamry KA, Jain RK. Polypyrrole nanoparticles-based soft actuator for artificial muscle applications. *RSC Advances.* 2019;9:39721-34.
  12. Inamuddin, Abbas Kashmery H. Polyvinylidene fluoride/sulfonated graphene oxide blend membrane coated with polypyrrole/platinum electrode for ionic polymer metal composite actuator applications. *Sci Rep.* 2019;9:9877.
  13. Rasouli H, Naji L, Hosseine MG. The influence of electrodeposited conducting polymer electrode structure on the actuation performance of muscle-like ionic actuators. *Sens Actuators A Phys.* 2018;279:204-15.
  14. Liu J, Li Y, Liang B, Du Y, Sun Z, Zhang P. Research on the synthesis and properties of PPY modified electrode IPMC. *IOP Conf Series Mater Sci Eng.* 2019;493:012048.
  15. Guo D, Wang L, Wang X, Xiao Y, Wang C, Chen L, et al. PEDOT coating enhanced electromechanical performances and prolonged stable working time of IPMC actuator. *Sens Actuators B Chem.* 2020;305:127488.
  16. Aabloo A, De Luca V, Di Pasquale G, Graziani S, Gugliuzzo C, Johanson U, et al. A new class of ionic electroactive polymers based on green synthesis. *Sens Actuators A Phys.* 2016;249:32-44.
  17. Khan A, Jain RK, Banerjee P, Inamuddin, Asiri AM. Soft actuator based on Kraton with GO/Ag/Pani composite electrodes for robotic applications. *Mater Res Express.* 2017;4:115701.
  18. Kazemi F, Naghieb SM, Mohammadpour Z. Multifunctional micro-/nanoscaled structures based on polyaniline: an overview of modern emerging devices. *Mater Today Chem.* 2020;16:100249.
  19. Lin T, Yu H, Wang L, Fahad S, Khan A, Naveed K, et al. A review of recent advances in the preparation of polyaniline-based composites and their electromagnetic absorption properties. *J Mater Sci.* 2021;56:5449-78.
  20. Beigi F, Mousavi MSS, Manteghi F, Kolahdouz M. Doped nafion-layered double hydroxide nanoparticles as a modified ionic polymer metal composite sheet for a high-responsive humidity sensor. *Appl Clay Sci.* 2018;166:131-6.
  21. Arnold AM, Su J, Sabolsky EM. Influence of environmental conditions and voltage application on the electromechanical performance of Nafion-Pt IPMC actuators. *Smart Mater Struct.* 2022;31:115031.
  22. Patel SN, Mukherjee S. Manufacturing, characterization and experimental investigation of the IPMC shoe energy harvester. *J Braz Soc Mech Sci Eng.* 2022;44:42.
  23. Qin Q, Tao J, Yang Y. Preparation and characterization of polyaniline film on stainless steel by electrochemical polymerization as a counter electrode of DSSC. *Synth Met.* 2010;160:1167-72.
  24. Maldonado-Larios L, Mayen-Mondragón R, Martínez-Orozco RD, Páramo-García U, Gallardo-Rivas NV, García-Alamilla R. Electrochemically-assisted fabrication of titanium-dioxide/polyaniline nanocomposite films for the electroremediation of congo red in aqueous effluents. *Synth Met.* 2020;268:116464.
  25. Li L, Liu H, Li B, Guo Y, Qing L, Wang B. Design and construction of polyaniline/reduced graphene oxide three-dimensional dendritic architecture on interdigital electrode for sensitive detection nitrite. *Macromol Res.* 2020;28(5):455-64.
  26. Vinodh R, Deviprasath C, Gopi CVVM, Kummara VGR, Atchudan R, Ahamad T, et al. Novel 13X Zeolite/PANI electrocatalyst for hydrogen and oxygen evolution reaction. *Int J Hydrogen Energy.* 2020;45:28337-49.
  27. Košiček KM, Kvastek K, Horvat-Radošević V. Hydrogen evolution on Pt and polyaniline modified Pt electrodes - a comparative electrochemical impedance spectroscopy study. *J Solid State Electrochem.* 2016;20:3003-13.
  28. Djara R, Lacour M-A, Merzouki A, Cambedouzou J, Cornu D, Tingry S, et al. Iridium and ruthenium modified polyaniline polymer leads to nanostructured electrocatalysts with high performance regarding water splitting. *Polymers (Basel).* 2021;13:190.
  29. Li J, Tian A, Wang X, Zhai Z, Zhang X, Feng B, et al. Dendrite growth and performance of self-healing composite electrode IPMC driven by  $\text{Cu}^{2+}$ . *ACS Omega.* 2022;7:17575-82.
  30. Zhang X, Yu S, Li M, Zhang M, Zhang C, Wang M. Enhanced performance of IPMC actuator based on macroporous multilayer MCNTs/Nafion polymer. *Sens Actuators A Phys.* 2022;339:113489.
  31. Lee K, Byun JY, Shin H, Kim SH. A high-performance supercapacitor based on polyaniline-nanoporous gold. *J Alloys Compd.* 2019;779:74-80.
  32. Korent A, Soderžnik KŽ, Šturm S, Rožman KŽ. A correlative study of polyaniline electropolymerization and its electrochromic behavior. *J Electrochem Soc.* 2020;167:106504.
  33. Belgherbi O, Chouder D, Saeed MA. Elaboration and characterization of ITO electrode modified by transition metal dispersed into polyaniline thin films. *Optik (Stuttg).* 2018;171:589-99.
  34. Sayah A, Habelhames F, Bahloul A, Boudjadi A. The effect of electrodeposition applied potential on the electrochemical performance of polyaniline films. *J Mater Sci Mater Electron.* 2021;32:10692-701.
  35. Sayah A, Habelhames F, Bahloul A, Nessark B, Bonnassieux Y, Tendelier D, et al. Electrochemical synthesis of polyaniline-exfoliated graphene composite films and their capacitance properties. *J Electroanal Chem (Lausanne).* 2018;818:26-34.
  36. Cruz-Silva R, Nicho ME, Reséndiz MC, Agarwal V, Castellón FF, Fariás MH. Electrochemical polymerization of an aniline-terminated self-assembled monolayer on indium tin oxide electrodes and its effect on polyaniline electrodeposition. *Thin Solid Films.* 2008;516:4793-802.
  37. Nautiyal A, Cook JE, Zhang X. Tunable electrochemical performance of polyaniline coating via facile ion exchanges. *Prog Org Coat.* 2019;136:105309.
  38. Mrad M, Amor YB, Dhoubi L, Montemor F. Electrochemical study of polyaniline coating electropolymerized onto AA2024-T3 aluminium alloy: physical properties and anticorrosion performance. *Synth Met.* 2017;234:145-53.
  39. Qin Q, He F, Zhang W. One-step electrochemical polymerization of polyaniline flexible counter electrode doped by graphene. *J Nanomater.* 2016;2016:1076158.
  40. Ye YJ, Huang ZH, Song Y, Geng JW, Xu XX, Liu XX. Electrochemical growth of polyaniline nanowire arrays on graphene sheets in partially exfoliated graphite foil for high-performance supercapacitive materials. *Electrochim Acta.* 2017;240:72-9.
  41. Gamero-Quijano A, Karman C, Vilà N, Herzog G, Walcarius A. Vertically aligned and ordered one-dimensional mesoscale polyaniline. *Langmuir.* 2017;33:4224-34.
  42. Gonçalves R, Tozzi KA, Saccardo MC, Zuquello AG, Scuracchio CH. Nafion-based ionomeric polymer/metal composites operating in the air: theoretical and electrochemical analysis. *J Solid State Electrochem.* 2020;24:1845-56.

43. Guo D, Wang L, Wang X, Xiao Y, Wang C, Chen L, et al. PEDOT coating enhanced electromechanical performances and prolonged stable working time of IPMC actuator. *Sens Actuators B Chem.* 2020;305:127488.
44. Sasi S, Krishna CA, Sugunan SK, Chandran A, Nair PR, Subramanian KRV, et al. Low cost, high efficiency flexible supercapacitor electrodes made from areca nut husk nanocellulose and silver nanoparticle embedded polyaniline. *RSC Advances.* 2021;11:29564-75.
45. Das NC, Rathod YU, Pandit VU, Gurnule WB. Studies of chelation ion-exchange properties of copolymer resin derived from 1,5-diaminonaphthalene, 2,4-dihydroxy-propiofenone and formaldehyde. *Mater Today Proc.* 2022;53:80-5.
46. Chen X, Chen Y, Shen Z, Song C, Ji P, Wang N, et al. Self-crosslinkable polyaniline with coordinated stabilized CoOOH nanosheets as a high-efficiency electrocatalyst for oxygen evolution reaction. *Appl Surf Sci.* 2020;529:147173.
47. Mishra PA, Rathod YU, Pandit VU, Gurnule WB. Thermal degradation studies of 2-hydroxy-4-methoxy acetophenone, guanidine and formaldehyde copolymer. *Mater Today Proc.* 2022;53:86-90.
48. Luqman M, Shaikh H, Anis A, Al-Zahrani SM, Hamidi A, Inamuddin. Platinumcoated silicotungstic acidsulfonated polyvinyl alcoholpolyaniline based hybrid ionic polymer metal composite membrane for bending actuation applications. *Sci Rep.* 2022;12:4467.
49. Hao Y, Sani LA, Ge T, Fang Q. Phytic acid doped polyaniline containing epoxy coatings for corrosion protection of Q235 carbon steel. *Appl Surf Sci.* 2017;419:826-37.
50. Niu L, Li Q, Wei F, Chen X, Wang H. Electrochemical impedance and morphological characterization of platinum-modified polyaniline film electrodes and their electrocatalytic activity for methanol oxidation. *J Electroanal Chem (Lausanne).* 2003;544:121-8.
51. Ismail HK, Alesary HF, Juma JA, Hillman AR, Ryder KS. A comparative study of the formation, and ion and solvent transport of polyaniline in protic liquid-based deep eutectic solvents and aqueous solutions using EQCM. *Electrochim Acta.* 2022;418:140348.
52. Li Y, Zhou M, Xia Z, Gong Q, Liu X, Yang Y, et al. Facile preparation of polyaniline covalently grafted to isocyanate functionalized reduced graphene oxide nanocomposite for high performance flexible supercapacitors. *Colloids Surf A Physicochem Eng Asp.* 2020;602:125172.
53. Sun Z, Du S, Zhang D, Song W. Influence of pH and loading of PANI on electrochemical and electromechanical properties for high-performance renewable soft actuator with nano-biocomposite electrode. *React Funct Polym.* 2019;139:102-11.
54. Alamry KA, Khan A, Hussein MA, Alfaifi SY. Sensitive electrochemical detection of toxic nitro-phenol in real environmental samples using enzymeless oxidized-carboxymethyl cellulose-sulfate/sulfated polyaniline composite based electrode. *Microchem J.* 2022;172:106902.
55. Surana K, Singh PK, Bhattacharya B, Verma CS, Mehra RM. Synthesis of graphene oxide coated Nafion membrane for actuator application. *Ceram Int.* 2015;41:5093-9.
56. Khan A, Inamuddin, Jain RK. Easy, operable ionic polymer metal composite actuator based on a platinum-coated sulfonated poly(vinyl alcohol)-polyaniline composite membrane. *J Appl Polym Sci.* 2016;133:33.
57. Khan A, Jain RK, Banerjee P, Ghosh B, Inamuddin, Asiri AM. Development, characterization and electromechanical actuation behavior of ionic polymer metal composite actuator based on sulfonated poly(1,4-phenylene ether-ether-sulfone)/carbon nanotubes. *Sci Rep.* 2018;8:9909.
58. Yang L, Zhang D, Zhang X, Tian A, Wang X. Models of displacement and blocking force of ionicpolymer metal composites based on actuation mechanism. *Appl Phys, A Mater Sci Process.* 2020;126:365.
59. Yang L, Zhang D, Zhang X, Tian A. Prediction of the actuation property of cu ionic polymer-metal composites based on backpropagation neural networks. *ACS Omega.* 2020;5:4067-74.